SIMULATING THE EFFECTS OF SUBSTRATE PRE-HEATING ON THE FINAL STRUCTURE OF STEEL PARTS BUILT BY LASER POWDER DEPOSITION

L. Costa[1], R. Vilar[1] and T. Réti[2]
[1] DEMat, IST, Av. Rovisco Pais, 1049-001 Lisboa, Portugal
[2] Szechenyi Istvan University, Egyetem ter 1., H- 9026 Györ, Hungary

Abstract

Tool steel parts built by laser powder deposition often present a heterogeneous distribution of properties caused by the complex structural transformations that occur during the deposition process. A model describing these transformations has been developed. It couples finite element heat transfer calculations with transformation kinetic theory to predict the final microstructure and properties of the material and their variation across a laser powder deposited part.
Pre-heating is often used to reduce the residual stresses and the risk of thermal distortion and cracking. However, this changes the heat transfer conditions and affects the final microstructure and properties. In this work the proposed model was used to evaluate the effects of substrate pre-heating on the final hardness distribution. The results show that the final hardness depends considerably on the initial temperature of the substrate.

Introduction

Multilayer laser powder deposition (LPD) is being developed since a few years for rapid manufacturing [1-9] and rapid tooling [10-13] applications. In this process parts are built by overlapping consecutive layers of a laser melted material (Fig. 1). Since cooling involves heat conduction to the bulk, the material in each layer will undergo successive thermal cycles as new layers are added. These short duration thermal cycles can induce solid-state transformations in the previously deposited layers that lead to progressive modification of their microstructure and properties. In the case of tool steels, these transformations will ultimately lead to a final microstructure that typically presents two distinct regions [11, 14-17]: an upper region of untempered martensite with high hardness and a lower region of tempered martensite with lower hardness (Fig. 1). This behavior has been observed for different materials (AISI 420, AISI P20 and AISI H13 tool steels) and wide range of processing conditions. Although the advantages of LPD are widely recognized, the existence of such heterogeneity in the properties of manufactured parts might limit its industrial applications. Thus, it is important to understand the origin of this heterogeneity and to develop tools that will allow minimizing it by optimizing the LPD parameters. The appearance of these two distinct regions was explained qualitatively by Griffith et al. [18] by using equilibrium phase diagram information to relate the local microstructure in the deposited parts with the corresponding peak temperature, measured experimentally. Softening in the lower layers was explained [11, 14-17] by tempering of martensite due to reheating of the material during the deposition of subsequent layers. Brooks et al. [19] proposed a time-temperature parameter that relates the hardness changes' due to tempering to the local thermal history. The authors applied this parameter to experimental data and showed that it accounts for the observed decrease of hardness. Although successful in explaining experimental observations, neither of the previous methods can be used for process optimization, in particular, to avoid softening of the lower layers. Obviously, the task of choosing a deposition strategy and processing parameters that would lead to parts with consistent material properties would be made

easier if these characteristics could be accurately predicted, using an adequate computational model. The approaches suggested by Griffith et al. [18] and Brooks et al. [19] have limited prediction ability because they do not calculate the time-dependent temperature in the part and do not contemplate any means of quantifying the effects of the phase transformations that occur during deposition on the final microstructure and properties of the part. The thermal history will differ from point to point in the part and it will depend on the deposition parameters, build-up strategy, substrate pre-heating temperature and geometry of the part being built. As a result, the type and extent of the solid-state phase transformations induced by the thermal field in the part may vary from point to point, thus leading to the complex distribution of microstructure and properties observed experimentally. Therefore, predicting the final microstructure distribution within the part requires models describing the time evolution of the temperature distribution in the part, the solidification structure formation mechanisms, the solid-state phase transformations that might occur and their kinetics. If material properties are to be assessed, then an adequate model relating properties to microstructure and thermal history must also be considered.

The thermo-kinetic model of multilayer laser powder deposition presented in this paper couples finite element heat transfer calculations with transformation kinetic data to simulate the microstructural transformations that occur in the material during deposition. Semi-empirical microstructure-properties relationships are used to evaluate the final hardness distribution in the part. Initial results [20] obtained by application of this model show that the proportion of tempered martensite present in the final part can be substantially reduced under conditions that promote heat accumulation in the part during the build-up process. This fact suggests that substrate pre-heating might have a significant effect on the final structure of tool steel parts built by LPD. This possibility was investigated for the case of a ten-layer wall of AISI 420 tool steel (0.33 %C, 13.5 %Cr) built by LPD.

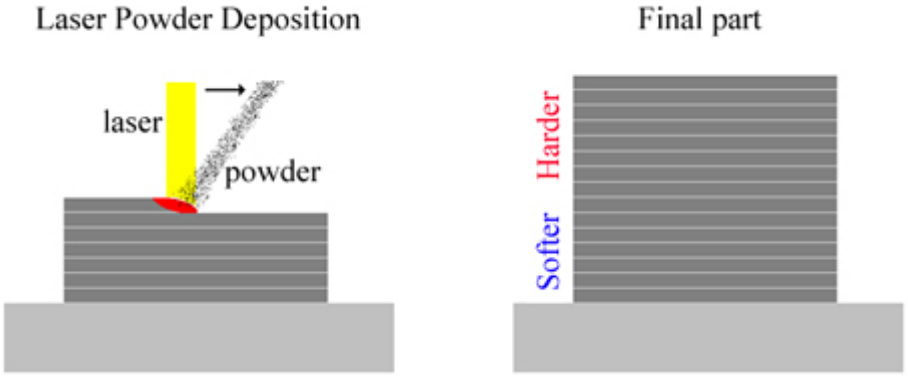

Figure 1. During laser powder deposition a material in powder form is injected into a laser beam and melted simultaneously with a thin layer of the substrate to form a continuous track of material. Partial overlapping of individual tracks in a suitable pattern produces a continuous layer of material. By overlapping such layers, three-dimensional objects are generated. In general, tool steel parts built by LPD will present an upper region of untempered martensite and a lower region of tempered martensite, with high and low hardness respectively.

Thermo-kinetic finite element model

The properties of a laser melted and resolidified material depend, on one hand, of the solidification path, and, on the other hand, on the solid-state transformations that might occur during cooling. In the case of LPD, transformations induced by the consecutive short-duration thermal cycles generated each time that a new layer is added to the part must also be considered.

The solidification mechanisms and solid-state transformations that occur in laser processed tool steels were studied in detail by Colaço and Vilar [21-23]. In particular, these authors showed that, due to the fast solidification rate observed in laser processing, the precipitation of austenite is kinetically favored to the precipitation of ferrite, the equilibrium solidification phase in tool steels containing substantial proportions of carbide forming alloying elements [22]. Moreover, this austenite can be stabilized by the very fine dendritic size and large supersaturation in alloying elements, resulting in an abnormally large proportion of austenite being retained at room temperature [21]. The austenite and martensite existing in the part after cooling down to room temperature evolve when the material is reheated, leading to complex tempering microstructures. The transformations observed during tempering were studied by Colaço et al. [23] for AISI 420 tool steel. Martensite decomposes into ferrite and cementite ($M \rightarrow \alpha + M_3C$) in the temperature range 200 to 350 ºC. As the temperature rises above 500 ºC, precipitation reactions leading to the formation of M_7C_3 and $M_{23}C_6$ carbides are activated, while M_3C dissolves progressively in the matrix, providing carbon for the precipitation of the alloy carbides. When the temperature exceeds 575 ºC retained austenite destabilizes and transforms partially or totally into lath type martensite during subsequent cooling [23]. A tempering hardness peak similar to the secondary hardening peak is observed, but at higher temperature than the secondary hardening temperature (600 ºC as compared to 500 ºC). The hardening mechanisms in tempering of laser melted steels are also different from those occurring in conventional tempering [23], because the major contribution to the material hardness increase is the transformation of retained austenite into martensite and not precipitation hardening.

The solidification microstructure can, to some extent, be predicted on the basis of existing solidification models [22, 24, 25], provided that reliable values for the relevant physical and thermodynamic properties are available. As to the prediction of the solid-state transformations, several relevant models were previously described in the literature by Johnson and Mehl [26] and Avrami [27-29], Koistinen and Marburger [30], Leblond and Devaux [31], Denis et al. [32], Pont et al. [33], Oddy et al. [34], Jones and Bhadeshia [35], Reti et al. [36]. Given the material microstructure, properties such as hardness can be estimated using semi-empirical relations proposed by Venugopalan and Kirkaldy [37], Reti et al. [38], Brooks et al. [19] and Bhadeshia [39]. The application of these models requires knowledge of specific fitting constants adequate to the particular processing conditions and materials used.

The laser powder deposition model takes into consideration phenomena such as mass and heat transfer and phase transformations. These phenomena are described by a set of coupled equations that has no analytical solutions and, therefore, can only be solved using numerical methods. In the present work, heat transfer calculations were performed using the ABAQUS finite element software package [40]. The temperature field (T=T(x,y,z,t)) in the part, calculated at each time instant as a function of the part shape and dimensions, boundary conditions, material properties and processing parameters, is used to predict the solidification microstructure and subsequent solid-state transformations, using semi-empirical relations to calculate the volume fractions of the resulting phases. It was assumed that the solidification structure consists entirely of primary austenite. The material hardness at each point was calculated on the basis of empirical structure-properties relationships. The solution of each iteration of the heat transfer calculations was also used to update the values of the density, thermal conductivity and specific heat at each point, calculated as weighed averages of the properties of the individual phases using the volume fractions of these phases as weights.

Heat transfer calculations

To calculate the temperature distribution in the part during the deposition process using the finite element method, the geometry of the part must be represented by a mesh of finite elements that changes over time to simulate the continuous addition of material. This time-dependent problem was solved sequentially, as a series of constant geometry problems (called steps), linked together by introducing the output of problem **n** as the initial condition for problem **n+1**. This stepwise approach is presented in Fig. 2. At the beginning of each step a new group of finite elements is activated and the boundary conditions updated according to the newly exposed surfaces. The total number of elements effectively activated at the beginning of each step is calculated considering the volume of material added during the corresponding time interval. This volume is a function of the powder mass flow rate, powder use efficiency and material density. The density, ρ, specific heat, c_p, and thermal conductivity, k, are all both phase and temperature dependent (Table 1). Latent heats associated to phase transformations are taken into account by an internal heat source term, Γ, of the heat conduction equation (Eq. 1). It was assumed that the base material was initially at temperature $T_{substrate}$ (Eq. 2a). Based on previous theoretical results of Neto and Vilar [41], who showed that the energy absorbed by the powder particles as they fly across the laser beam can be sufficient for them to reach the liquidus temperature before entering the melt pool, it was assumed that the finite elements which are activated at the beginning of each deposition step are at the liquidus temperature (Eq. 2b). The boundary conditions (Eq. 3a) take into consideration heat losses due to convection and radiation. Assuming that the laser beam is Gaussian, laser heating was simulated by applying a surface heat flux described by Eq. 3b. This heat flux depends on the laser beam power, P, laser beam radius, r_L, and surface reflectivity, R. Surface emissivity and Stefan-Boltzmann constant are represented by ε and σ respectively, while h represents the convective heat transfer coefficient and T_0 the sink temperature.

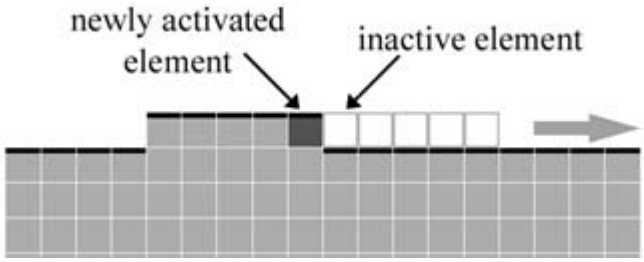

Figure 2. Finite element analysis of laser powder deposition performed using a stepwise approach. The addition of material was modeled by activating a new group of finite elements at the beginning of each step.

$$\rho\, c_P \frac{\partial T}{\partial t} = div \cdot (k\ grad\ T) + \Gamma\ . \tag{1}$$

Initial conditions:

Finite elements of the substrate: $$T(x,y,z,t=0) = T_{substrate}\ . \tag{2a}$$

Newly active finite elements: $$T(x,y,z,t_{activation}) = T_{Liquidus}\ . \tag{2b}$$

Boundary conditions:

$$k\,(\nabla T \cdot \vec{n})\,|_{\Omega} = h\,(T - T_0)\,|_{\Omega} + \varepsilon\,\sigma\,(T^4 - T_0^4)\,|_{\Omega} - F_{Laser}\,|_{\Omega\,Laser}\ . \tag{3a}$$

Surface heat flux term simulating a Gaussian laser beam:

$$F_{Laser} = F_0 \, e^{-2 \cdot r^2 / r_L^2}, \qquad F_0 = (1-R) \cdot \frac{2 \cdot P}{\pi \cdot r_L^2}. \tag{3b}$$

Modeling of solid-state phase transformations

The solidification of laser processed AISI 420 tool steel leads to the formation of austenite with a dendritic structure [22]. In the present work this phase was considered to be chemically homogeneous. Due to the high cooling rate observed in LPD, diffusive austenitic transformations are suppressed during cooling down to room temperature and austenite may only transform into martensite. The martensitic transformation starts as soon as the temperature drops below the martensite start temperature, Ms, and the volume fraction of martensite increases with the undercooling. The volume fraction of martensite, f_M, was calculated using the Koistinen and Marburger equation [30] (Eq. 4), where $f_{\gamma 0}$ is the initial volume fraction of austenite. The Ms temperature was calculated from the chemical composition of the steel, using Andrews' equation [42] (Eq. 5), where the chemical element designations refer to concentrations in wt. %. For a AISI 420 steel with 0.33 %C and 13.5 %Cr, Ms = 160 ºC.

$$f_M = 1 - f_{\gamma_0} \cdot \Phi(T), \qquad \Phi(T) = \begin{cases} 1 & ,if \;\; T \geq Ms \\ \exp\left(-0.011 \cdot (Ms - T)\right) & ,if \;\; T < Ms \end{cases}, \tag{4}$$

$$\text{Ms} = 512 - 453 \times (\%\text{C}) - 15 \times (\%\text{Cr}). \tag{5}$$

If the material is reheated and its temperature exceeds Ac_1, ferrite formed during tempering of martensite will transform into austenite, which will progressively dissolve the carbides. The volume fraction of austenite increases with temperature, to reach 100% at the Ac_3 temperature. In the model this variation was assumed to be linear and austenite was considered to be chemically homogeneous. Taking into consideration the high heating rates characteristic of the LPD process, Ac_1 and Ac_3 will present hysteresis, an effect that was taken into account by making Ac_1 and Ac_3 equal to 875 and 1015 ºC, respectively, based on experimental results of Rose et al. [43]. It was also assumed that a martensitic transformation will only occur if new austenite is formed during reheating, thus neglecting destabilization of retained austenite during tempering and its transformation into martensite upon subsequent cooling [23].

Hardness prediction

The hardness of the material was assumed to be equal to the weighed average of the hardnesses of individual phases (Eq. 6), where f_γ is the volume fraction of austenite and H_γ and $H_{M'}$ are the hardness of austenite (280 HV) and tempered martensite, respectively. The hardness of tempered martensite was calculated using a model due to Reti et al. [38]. These authors showed that the variation of hardness due to anisothermal tempering can be estimated using Eq. 7, where H_0 is the hardness of fresh martensite, R the universal gas constant and A and m fitting constants. Since in the present case several competitive reactions occur simultaneously, the activation energy, Q, in Eq. 7 was replaced by an effective activation energy, as suggested by Mittemeijer [44]. The values of the parameters for AISI 420 steel were calculated from data collected from isothermal tempering experiments performed by the authors, leading to H_0 = 658 HV, A = 1300 HV/s, m = 0.055 and the effective activation energy values presented in Table 2.

$$H = f_\gamma \cdot H_\gamma + (1 - f_\gamma) \cdot H_{M'}, \tag{6}$$

$$H_{M'} = H_0 - A \cdot \left[\int_0^t e^{-Q/R \times T(t)} \cdot dt \right]^m . \tag{7}$$

Influence of the pre-heating temperature on microstructure and properties of tool steel parts built by laser powder deposition

The influence of pre-heating temperature on the final structure of tool steel parts built by LPD was analyzed for the following initial and boundary conditions: $T_{substrate} = T_{0\ (substrate)}$ = 0, 27, 60, 90, 120, 150, 165 ºC. The analysis was performed for a ten-layer wall of AISI 420 tool steel, built by overlapping single tracks of material, each with a length of 10.0 mm, a thickness of 0.5 mm and a width of 1.0 mm (Fig. 3). The idle time between the deposition of consecutive layers, Δt, was 10 s and the deposition parameters were: scanning speed = 20 mm/s, powder feed rate = 0.1 g/s and powder use efficiency = 78%. For a track width of 1.0 mm and these processing parameters two cubic elements, each with 0.5^3 mm^3, must be activated every 25 ms. The initial temperature of the newly active elements was 1450 ºC. A substrate of the same steel, quenched and double tempered for 1 hour at 200 ºC, with an initial microstructure of ferrite and carbides and a hardness of 560 HV, was assumed. The Gaussian laser beam was focused into a spot with 3 mm diameter, measured at e^{-2} of maximum intensity. Based on preliminary calculations, an absorbed laser beam power P' = (1-R)·P of 325 W was used to create an adequately sized melt pool. At the end of the deposition process, the entire part was allowed to reach room temperature, set at 27 ºC.

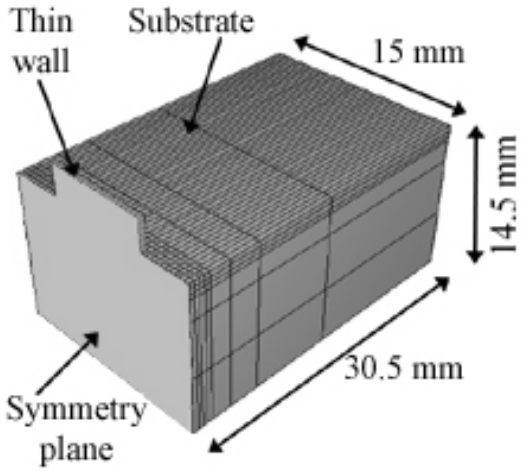

Figure 3. Finite element mesh used to simulate multilayer LPD of a 10 layer wall. A denser mesh of elements was used where higher thermal gradients are expected. A symmetry plane exists if the wall is built up along the mid-plane of the base material. In this case, only ½ of the global problem has to be solved if a zero heat flux condition is imposed along the symmetry plane.

Results

The influence of cumulative heat cycles on microstructural transformations and hardness changes' can be observed in the graph presented in Fig. 4. The data concerns the mid-point of layers 1, 5 and 9, with the substrate initially at room temperature ($T_{substrate} = T_{0\ (substrate)} = 27$ ºC). The plotted data indicates that during the idle time, Δt, the material in each layer cools below Ms temperature before the deposition of a new layer, so austenite transforms to martensite (Fig. 5a). The deposition of layer p leads to austenitization of layer p-1 and intense tempering of martensite in layer p-2. On the contrary, the tempering effect in layer p-3 is negligible. Since martensite in the last two layers to be deposited does not undergo tempering, it presents high hardness, while lower layers present lower hardness due to tempering of martensite. The corresponding final hardness distribution, presented in Fig. 5b, is similar to those previously reported in the literature. When the substrate is pre-heated at 165 ºC, the temperature of the deposited material remains above the Ms temperature during the entire deposition process and a fully austenitic microstructure is preserved until the end of the deposition process (Fig. 6a). This austenite transforms into martensite after deposition, when the entire part cools down to room temperature, so the final part consists mostly of untempered martensite and some retained austenite and presents high hardness (Fig. 6b). Thus, if these processing conditions are used, the two-region structure can be avoided and the hardness distribution in the part is uniform.

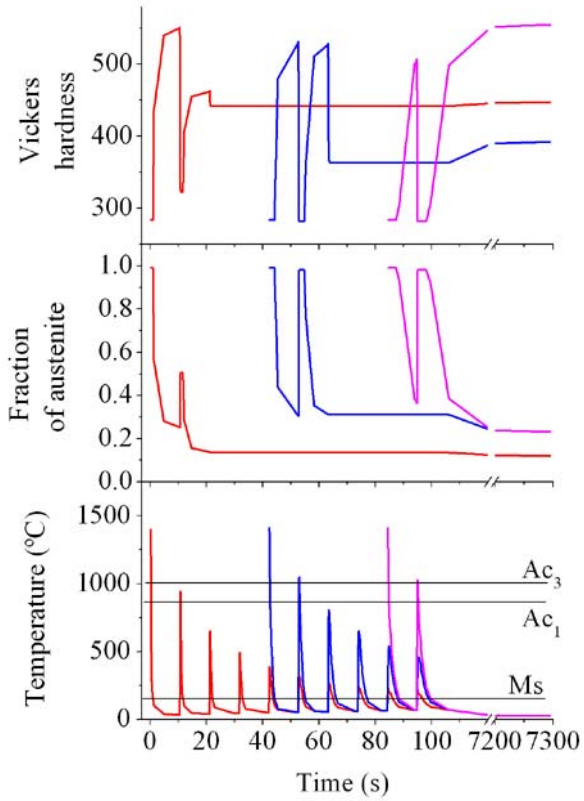

Figure 4. Layers 1, 5 and 9. $T_{substrate} = 27$ ºC. Time-evolution of temperature, fraction of austenite and hardness.

a) b)

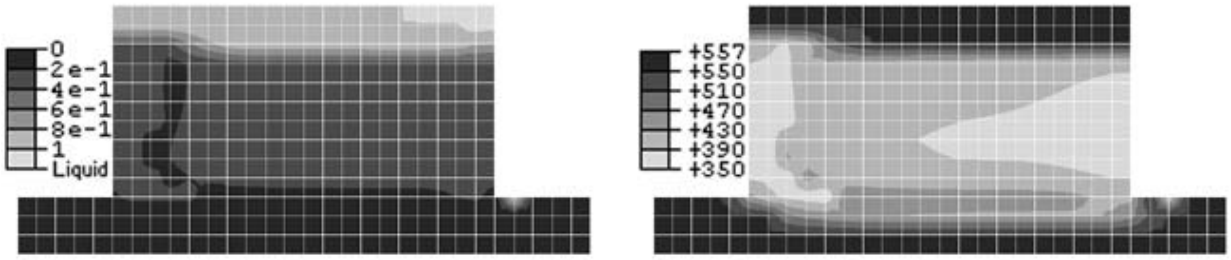

Figure 5. Symmetry plane of the part. $T_{substrate}$ = 27 ºC.
a) Fraction of austenite, at the end of the last deposition step; t = 95.2 s.
b) Vickers hardness distribution, after cooling to room temperature; t = 7300 s.

a) b)

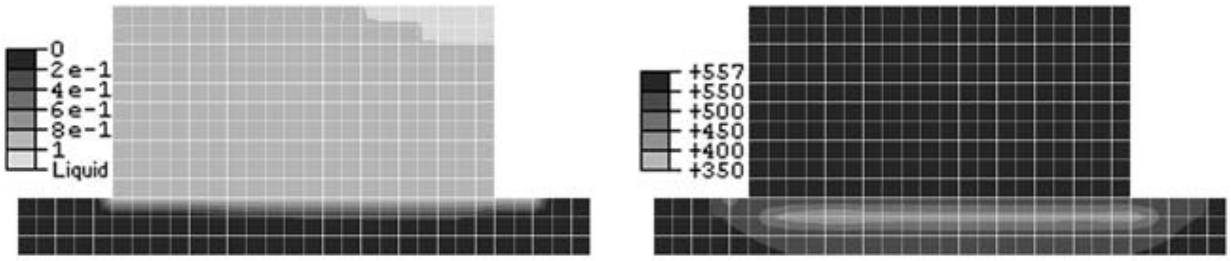

Figure 6. Symmetry plane of the part. $T_{substrate}$ = 165 ºC.
a) Fraction of austenite, at the end of the last deposition step; t = 95.2 s.
b) Vickers hardness distribution, after cooling to room temperature; t = 7300 s.

Between the extreme cases described previously, an entire range of possible structures presenting different proportions of tempered martensite may be obtained by varying the pre-heating temperature. As the initial temperature of the substrate is increased, the undercooling below Ms experienced by recently deposited material during the idle time, Δt, decreases and, as a consequence, the proportion of retained austenite increases. Since the hardness decrease due to martensite tempering is proportional to the volume fraction of martensite, higher pre-heating temperatures will eventually lead to harder parts and more uniform hardness distributions. This effect can be observed in Fig. 7, where the final hardness profile along the wall height is presented for several values of the pre-heating temperature. Independently of the pre-heating temperature, significant tempering occurs in the heat affected zone of the substrate, leading to a local hardness minimum.

The hardness distribution can also be modified by changing deposition parameters, as reported by Griffith et al. [15]. However, this approach may negatively affect other important aspects such as the build rate and the surface roughness. The results presented previously show that the pre-heating temperature can be used to manipulate the final structure and properties of parts, while deposition parameters such as laser beam power, powder feed rate and scanning speed can be adjusted as to optimize the build rate and surface roughness. Pre-heating the substrate has the additional advantage of reducing residual stresses and the consequent risks of thermal distortion and cracking.

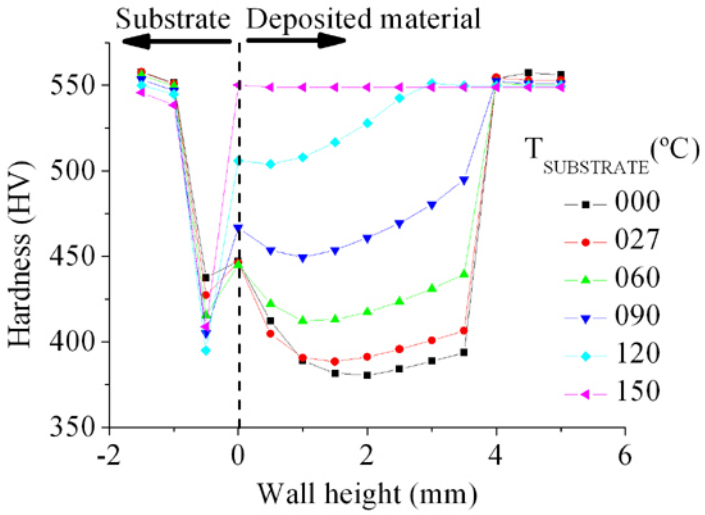

Figure 7. Vickers hardness along the wall height center line, for different values of $T_{substrate}$.

Conclusions

A thermo-kinetic model of multilayer laser powder deposition has been used to investigate the influence of substrate pre-heating on the microstructure and hardness distribution in tool steel parts built by laser powder deposition. The simulation results show that parts built on a substrate at room temperature often present a hard upper region containing mostly fresh martensite and some retained austenite and a softer lower region consisting of tempered martensite. On the contrary, when the substrate is pre-heated to an adequate temperature, near the Ms temperature, the temperature in the part remains higher than Ms until the end of the deposition process and an homogeneous martensitic structure having a uniformly high hardness is obtained. The results achieved confirm the potential and usefulness of using suitable physico-computational models and computer numerical techniques to investigate laser powder deposition.

Appendix

Table 1. Material properties used in the finite element analysis [45, 46].

Temperature [ºC]	-	27	300	600	800	900	1100	1300	1410	1425
Thermal conductivity [W/m·K]	M, α	43.1	36.7	30.1	-	-	-	-	-	-
	γ	15.0	18.0	21.7	25.1	26.8	28.9	32.8	-	34.0
Specific heat [J/kg·K]	M, α	485	574	654	-	-	-	-	-	-
	γ	535	568	603	632	-	-	760	750	-
Density [kg/m^3]	-	7750	-	-	-	-	-	-	-	-
Latent heat of fusion [kJ/kg]	-	-	-	-	-	-	-	-	-	250

M – martensite; α - ferrite; γ - austenite

Table 2. Values of effective activation energy, Q, for AISI 420 tool steel.

T [ºC]	20	300	400	500	600	700
Q [kJ/mol]	220	220	250	320	250	250

Acknowledgements

Lino Costa, gratefully acknowledges financial support from Fundação para a Ciência e Tecnologia (FCT), Fundação Luso-Americana para o Desenvolvimento (FLAD) and Instituto de Ciência e Engenharia de Materiais e Superfícies (ICEMS). The authors also acknowledge GRICES for financial support (project: Repairing of machine parts by laser cladding – Proj. 4.1.1 OMFB).

References

1. Koch, J.L. and J. Mazumder. *Rapid prototyping by laser cladding*. ICALEO. 1993: p. 556-565.
2. Lewis, G.K., et al. *Directed light fabrication*. ICALEO. 1994: p. 17-26.
3. Kreutz, E.W., et al., *Rapid prototyping with C02 laser radiation.* Appl. Surf. Sci., 1995. **86**: p. 310-316.
4. Gremaud, M., et al., *Laser metal forming: process fundamentals.* Surf. Eng., 1996. **12**(3): p. 251-259.
5. Griffith, M.L., et al. *Free form fabrication of metallic components using laser engineered net shaping (LENS)*. Solid Freeform Fabrication Symposium. 1996: p. 125-131.
6. Xue, L. and M.U. Islam, *Free-form laser consolidation for producing metallurgically sound and functional components.* J. Laser Appl., 2000. **12**(4): p. 160-165.
7. Arcella, F.G., D.H. Abbott, and M.A. House. *Titanium alloy structures for airframe application by the laser forming process*. AIAA structures, structural dynamics & materials conference. 2000.
8. Capshaw, B. *Improved performance for motorsports applications through laser powder deposition technology*. International Conference on Metal Powder Deposition for Rapid Manufacturing. 2002: p. 69-76.
9. Wu, X. and J. Mei, *Near net shape manufacturing of components using direct laser fabrication technology.* J. Mater. Process. Tech., 2003. **135**: p. 266-270.
10. Fessler, J.R., et al. *Laser deposition of metals for shape deposition manufacturing*. Solid Freeform Fabrication Symposium. 1996: p. 117-124.
11. Mazumder, J., et al., *The direct metal deposition of H13 tool steel for 3D components.* JOM, 1997. **49**(5): p. 55-60.
12. Atwood, C., et al. *Laser Engineered net shaping (LENS): a tool for direct fabrication of metal parts*. ICALEO. 1998: p. E1-E7.
13. Morgan, D., *New metal-fabrication application.* Industrial Laser Solutions, 2000. **15**(1): p. 8-10.
14. Link, G., *Layered manufacturing of laser deposited carbon steels*. PhD Thesis. 1999, Stanford University.
15. Griffith, M.L., et al. *Thermal behavior in the LENS process*. Solid Freeform Fabrication Symposium. 1998: p. 89-96.
16. Mazumder, J., A. Schifferer, and J. Choi, *Direct materials deposition: designed macro and microstructure.* Mater. Res. Innov., 1999. **3**: p. 118-131.
17. Chen, J.Y. and L. Xue. *Microstructural characteristics of laser-clad AISI P20 tool steel*. International surface engineering congress, IFHTSE congress. 2002: p. 198-205.

18. Griffith, M.L., et al. *Understanding the microstructure and properties of components fabricated by laser engineered net shaping (LENS)*. Solid Freeform and Additive Fabrication. 2000: p. 9-20.
19. Brooks, J., et al. *Microstructure and property optimization of LENS deposited H13 tool steel*. Solid Freeform Fabrication Symposium. 1999: p. 375-382.
20. Costa, L., et al., *Simulation of phase transformations in steel parts produced by laser powder deposition.* Mater. Sci. Forum, 2005. **473-474**: p. 315-320.
21. Colaço, R. and R. Vilar, *Effect of the processing parameters on the proportion of retained austenite in laser surface melted tool steels.* J. Mater. Sci. Lett., 1998. **17**: p. 563-567.
22. Colaço, R. and R. Vilar, *Phase selection during solidification of AISI 420 and AISI 440C tool steels.* Surf. Eng., 1996. **12**(4): p. 319-325.
23. Colaço, R. and R. Vilar, *Effect of laser surface melting on the tempering behaviour of DIN X42Cr13 stainless tool steel.* Scripta Mater., 1998. **38**(1): p. 107-113.
24. Kurz, W., B. Giovanola, and R. Trivedi, *Theory of microstructural development during rapid solidification.* Acta Metall., 1986. **34**(5): p. 823-830.
25. Rappaz, M., et al., *Analysis of solidification microstructures in Fe-Ni-Cr single-crystal welds.* Metall. Trans. A, 1990. **21**: p. 1767-1782.
26. Johnson, W.A. and R.F. Mehl, *Reaction kinetics in process of nucleation and growth.* Trans. AIME, 1939. **135**: p. 416-458.
27. Avrami, M., *Kinetics of phase change, part I: general theory.* J. Chem. Phys., 1939. **7**: p. 1103-1112.
28. Avrami, M., *Kinetics of phase change, part II: transformation time relations for random distribution of nuclei.* J. Chem. Phys., 1940. **8**: p. 212-224.
29. Avrami, M., *Kinetics of phase change, part III: granulation, phase change and microstructure.* J. Chem. Phys., 1941. **9**: p. 177-184.
30. Koistinen, D.P. and R.E. Marburger, *A general equation prescribing the extent of the austenite-martensite transformation in pure iron-carbon alloys and plain carbon steels.* Acta Metall., 1959. **7**: p. 59-60.
31. Leblond, J.B. and J.C. Devaux, *A new kinetic model for anisothermal metallurgical transformations in steels including effect of austenite grain size.* Acta Metall., 1984. **32**(1): p. 137-146.
32. Denis, S., D. Farias, and A. Simon, *Mathematical model coupling phase transformations and temperature evolutions in steels.* ISIJ International, 1992. **32**(3): p. 316-325.
33. Pont, D., et al. *Identification of a kinetic model for anisothermal metallurgical transformations in steels*. 2nd international symposium on inverse problems in engineering mechanics. 1994: p. 151-156.
34. Oddy, A.S., J.M. McDill, and L. Karlsson, *Microstructural predictions including arbitrary thermal histories, reaustenitization and carbon segregation effects.* Can. Metall. Quart., 1996. **35**(3): p. 275-283.
35. Jones, S.J. and H.K.D.K. Bhadeshia, *Kinetics of the simultaneous decomposition of austenite into several transformation products.* Acta Mater., 1997. **45**(1997): p. 2911-2920.
36. Reti, T., Z. Fried, and I. Felde, *Computer simulation of steel quenching process using a multi-phase transformation model.* Comp. Mater. Sci., 2001. **22**: p. 261-278.
37. Venugopalan, D. and J.S. Kirkaldy. *New relations for predicting the mechanical properties of quenched and tempered low alloy steels*. Hardenability concepts with applications to steels. 1977.

38. Réti, T., M. Gergely, and P. Tardy, *Mathematical treatment of non-isothermal transformations.* Mater. Sci. Tech., 1987. **3**: p. 365-371.
39. Bhadeshia, H.K.D.H. *Complex weldment properties: trends in predictive power*. 6th international conference on trends in welding research. 2002.
40. Hibbitt, et al., *ABAQUS manual*. 1999.
41. Neto, O.O.D. and R. Vilar, *Physical-computational model to describe the interaction between a laser beam and a powder jet in laser surface processing.* J. Laser Appl., 2002. **14**(1): p. 46-51.
42. Andrews, K.W., *Empirical formulae for the calculation of some transformation temperatures.* J. Iron Steel Inst., 1965. **203**: p. 721-727.
43. Rose, A., et al., *Atlas zur Warmebehandlung der stahle*. Vol. II. 1961: p. 239. Veralg Stahleisen M. B. H.
44. Mittemeijer, E.J., *Review: Analysis of the kinetics of phase transformations.* J. Mater. Sci. 1992. **27**: p. 3977-3987.
45. Totten, G., M. Howes, and T. Inoue, eds. *Handbook of residual stress and deformation of steel*. 2002: p. 3. ASM International.
46. Morwood, G.D., *Dimensional Changes of Investment Cast H13 Tool Steel*. PhD Thesis. 2000, The University of Queensland.